

## Article

# Highly Sensitive and Selective Dopamine Determination in Real Samples Using Au Nanoparticles Decorated Marimo-like Graphene Microbead-Based Electrochemical Sensors

Qichen Tian <sup>1,2,†</sup>, Yuanbin She <sup>1,†</sup>, Yangguang Zhu <sup>2</sup>, Dan Dai <sup>1,2</sup>, Mingjiao Shi <sup>2</sup>, Wubo Chu <sup>2,3,4</sup>, Tao Cai <sup>2,3,4</sup>, Hsu-Sheng Tsai <sup>5,6</sup>, He Li <sup>2,3,4</sup>, Nan Jiang <sup>2,3,4</sup>, Li Fu <sup>7</sup> , Hongyan Xia <sup>8,\*</sup>, Cheng-Te Lin <sup>2,3,4,\*</sup>  and Chen Ye <sup>2,3,4,\*</sup>

<sup>1</sup> College of Chemical Engineering, Zhejiang University of Technology, Hangzhou 310014, China

<sup>2</sup> Qianwan Institute, Ningbo Institute of Materials Technology and Engineering (NIMTE), Chinese Academy of Sciences, Ningbo 315201, China

<sup>3</sup> Center of Materials Science and Optoelectronics Engineering, University of Chinese Academy of Sciences, Beijing 100049, China

<sup>4</sup> Key Laboratory of Marine Materials and Related Technologies, Zhejiang Key Laboratory of Marine Materials and Protective Technologies, Ningbo Institute of Materials Technology and Engineering (NIMTE), Chinese Academy of Sciences, Ningbo 315201, China

<sup>5</sup> Laboratory for Space Environment and Physical Sciences, Harbin Institute of Technology, Harbin 150001, China

<sup>6</sup> School of Physics, Harbin Institute of Technology, Harbin 150001, China

<sup>7</sup> College of Materials and Environmental Engineering, Hangzhou Dianzi University, Hangzhou 310018, China

<sup>8</sup> State Key Laboratory for Mechanical Behavior of Materials, Xi'an Jiaotong University, Xi'an 710049, China

\* Correspondence: [hyxia0707@xjtu.edu.cn](mailto:hyxia0707@xjtu.edu.cn) (H.X.); [linzhengde@nimte.ac.cn](mailto:linzhengde@nimte.ac.cn) (C.-T.L.); [yechen@nimte.ac.cn](mailto:yechen@nimte.ac.cn) (C.Y.)

† These authors contributed equally to this work.



**Citation:** Tian, Q.; She, Y.; Zhu, Y.; Dai, D.; Shi, M.; Chu, W.; Cai, T.; Tsai, H.-S.; Li, H.; Jiang, N.; et al. Highly Sensitive and Selective Dopamine Determination in Real Samples Using Au Nanoparticles Decorated Marimo-like Graphene Microbead-Based Electrochemical Sensors. *Sensors* **2023**, *23*, 2870. <https://doi.org/10.3390/s23052870>

Academic Editor: Alfredo de la Escosura-Muñiz

Received: 24 January 2023

Revised: 21 February 2023

Accepted: 3 March 2023

Published: 6 March 2023



**Copyright:** © 2023 by the authors. Licensee MDPI, Basel, Switzerland. This article is an open access article distributed under the terms and conditions of the Creative Commons Attribution (CC BY) license (<https://creativecommons.org/licenses/by/4.0/>).

**Abstract:** A sensitive and selective electrochemical dopamine (DA) sensor has been developed using gold nanoparticles decorated marimo-like graphene (Au NP/MG) as a modifier of the glassy carbon electrode (GCE). Marimo-like graphene (MG) was prepared by partial exfoliation on the mesocarbon microbeads (MCMB) through molten KOH intercalation. Characterization via transmission electron microscopy confirmed that the surface of MG is composed of multi-layer graphene nanowalls. The graphene nanowalls structure of MG provided abundant surface area and electroactive sites. Electrochemical properties of Au NP/MG/GCE electrode were investigated by cyclic voltammetry and differential pulse voltammetry techniques. The electrode exhibited high electrochemical activity towards DA oxidation. The oxidation peak current increased linearly in proportion to the DA concentration in a range from 0.02 to 10  $\mu\text{M}$  with a detection limit of 0.016  $\mu\text{M}$ . The detection selectivity was carried out with the presence of 20  $\mu\text{M}$  uric acid in goat serum real samples. This study demonstrated a promising method to fabricate DA sensor-based on MCMB derivatives as electrochemical modifiers.

**Keywords:** dopamine determination; mesocarbon microbeads; gold nanoparticles; graphene nanowalls; electrochemical sensors

## 1. Introduction

Dopamine (DA) is distributed extensively in the central nervous system and peripheral tissues acting as a catecholamine neurotransmitter for message transfer, and it is involved in various important physiological functions including human metabolism, vasodilation, central nervous, motion control, as well as renal and hormonal systems [1–3]. DA is also a clinically important molecule in health care medicine, used in hypertension, bronchial asthma, cardiac surgery, and myocardial infarction [4]. The abnormal levels of DA in biological liquids and tissues are commonly related to several diseases and neurological disorders, like hypertension, schizophrenia, attention-deficit/hyperactivity, Parkinson's

disease, Alzheimer's disease, and Huntington's disease [5,6]. Due to the low concentration levels of DA in biological samples, usually in the range of several 10 s of nM, the development of reliable, accurate, and cost-effective sensing technology for the determination of DA with very high sensitivity and selectivity is essential in analytical and diagnostic applications [7,8]. Nowadays, in the field of DA detection, several analytical methods such as high-performance liquid chromatography, chemiluminescence, and capillary electrophoresis have been reported [9–11]. As the development of point of care testing (POCT) which is defined as medical diagnostic testing at/near the time and place of patient care [12,13], more requirements are raised for detection methods, including high sensitivity, low cost, ease-of-operation, and time efficiency, etc. Therefore, due to these competitive advantages, electrochemical analysis techniques have been regarded as a promising approach compatible with portable devices for the detection of electrochemically active DA molecules [14–16].

The most common electrode used for the recognition of electrochemically active compounds is the glassy carbon electrode (GCE) [7,17,18], which has a variety of advantages including inertness in a wide electrochemical window, chemical stability, and good electrical conductivity [19]. In order to further improve the sensing performance, several methods have been developed such as electrochemical activation [20], ultrasonication pretreatment [21], and surface modification with conductive nanomaterials [22–24]. Among them, the surface modification route has attracted a great deal of attention from academia and has become a rapidly growing research field, especially for biosensing applications [25–28]. In recent years, a variety of nanomaterials, such as nanoparticles (noble metals, transition metals, oxides, etc.) [29–31], nanotubes or nanofilaments (carbon nanotubes, noble metals, oxides, etc.) [32–34], and 2D materials (graphene, MXene, MoS<sub>2</sub> nanosheets, etc.) [35–37], have been reported as nanomodifiers to boost the sensitivity of GCE towards DA detection. One of the most well-known 2D materials, graphene, which is composed of sp<sup>2</sup>-hybridized carbon atoms packed into a honeycomb lattice [38], has a strong interaction with adsorbed biomolecules and thus shows superior performance to improve the properties of DA sensors compared to other nanomaterials [7,39,40] because of its high specific surface area (up to 800 m<sup>2</sup> g<sup>-1</sup>) [41], excellent electrical conductivity ( $\approx 2200$  S cm<sup>-1</sup>) [42], and diverse defects/functional groups with enhanced electrocatalytic activity [43].

In general, graphene sheets and their derivatives including graphene oxide (GO) and reduced graphene oxide (rGO) used for electrochemical modifiers, can be massively and economically produced by exfoliation of graphite using the Hummers method, ball milling, and liquid phase sonication [44–46]. Yang et al. fabricated rGO-modified electrodes through drop-casting of GO dispersion on the GCE surface followed by electrochemical reduction, showing the sensing performance of DA with a linear range of 0.5–60  $\mu$ M and a low detection limit of 0.5  $\mu$ M [47]. Ping et al. developed a screen-printed graphene electrode using rGO ink chemically reduced by a mixture of hydrazine and ammonia solution for selective detection of DA, achieving a linear range of 0.5–2000  $\mu$ M and a detection limit of 0.12  $\mu$ M [48]. Noticeably, the sensitivity of graphene-modified electrodes reported above still need improvement for real sample analysis, since the basal level of DA concentration in human serum or plasma can be very low (in the range of 1 nM–1  $\mu$ M) [18]. This limitation is because of the unavoidable formation of graphene agglomerates on the modified electrodes during the drying step when prepared by conventional drop casting, based on the strong  $\pi$ - $\pi$  interactions between graphene sheets [49,50], thus leading to a significant reduction of the effective area between graphene and biomolecules, as well as the degradation of the sensitivity of DA sensors [51].

In this work, we synthesized a unique marimo-like structure consisting of graphene layers on the surface of commercial mesocarbon microbeads (MCMB) for the highly sensitive determination of DA molecules, through the proposed self-exfoliation process. MCMB is the spherical graphite particle synthesized from petroleum pitch with an average diameter of 10 s micrometers and high electrical conductivity, having been a commonly

used material for lithium-ion batteries [52]. However, so far there is no report on the use of MCMB for applications in electrochemical sensors owing to the very low specific surface area ( $1.0\text{--}1.5\text{ m}^2\text{ g}^{-1}$ ) [53]. Instead, in our study, graphene layers were partially exfoliated from the MCMB surface to form a marimo-like structure at  $1000\text{ }^\circ\text{C}$  with KOH for increasing the electroactive area, meanwhile eliminating the agglomeration behavior of drop-casted graphene electrodes. In addition, the decoration of the graphene surface with noble metal nanoparticles (NP) has been proven to be an efficient approach to improve the electrochemical sensitivity of DA sensors based on their excellent electroactivity and biocompatibility [54,55]. As a result, the GCE modified with marimo-like graphene (MG) microbeads for DA determination exhibits a wide dynamic range of  $0.2\text{--}100\text{ }\mu\text{M}$  and a limit of detection (LOD) of  $0.15\text{ }\mu\text{M}$ , and can be further enhanced to have a linear range of  $0.02\text{--}10\text{ }\mu\text{M}$  and a LOD of  $0.016\text{ }\mu\text{M}$  ( $16\text{ nM}$ ) with the decoration of Au nanoparticles (Au NP). Moreover, the fabricated sensors exhibit good repeatability and specificity toward real sample analysis. To the best of our knowledge, this study is the first to report on sensing applications using MCMB derivatives as electrochemical modifiers.

## 2. Materials and Methods

### 2.1. Chemicals

Phosphate buffer solution ( $10\times$  PBS, containing  $137\text{ mM NaCl}$ ,  $102.7\text{ mM KCl}$ ,  $8.1\text{ mM Na}_2\text{HPO}_4$ , and  $1.8\text{ mM KH}_2\text{PO}_4$ ),  $\text{H}_2\text{SO}_4$ , KOH, NaCl, KCl, ascorbic acid ( $\text{C}_6\text{H}_8\text{O}_6$ ), uric acid (UA,  $\text{C}_5\text{H}_4\text{N}_4\text{O}_3$ ), and glucose ( $\text{C}_6\text{H}_{12}\text{O}_6$ ) were purchased from Sinopharm Chemical Reagent Co., Ltd. (Shanghai, China). Dopamine (DA, 4-(2-aminoethyl)-pyrocatecho hydrochloride,  $\text{C}_8\text{H}_{12}\text{ClNO}_2$ ) was purchased from Shanghai Aladdin Biochemical Technology Co., Ltd. (Shanghai, China).  $\text{HAuCl}_4\cdot 3\text{H}_2\text{O}$  was purchased from SigmaAldrich Trading Co., Ltd. (Shanghai, China). All chemical reagents were analytical grade without further purification. Mesocarbon microbeads (MCMB) were purchased from Tianjin BTR New Energy Technology Co., Ltd. (Tianjin, China). Goat serum was purchased from Sangon Biotech Co., Ltd. (Shanghai, China). Milli-Q deionized water (DI water,  $\approx 18.2\text{ M}\Omega\text{ cm}$ ) was extensively utilized in our experiments.

### 2.2. Fabrication of Au NP/Marimo-like Graphene Electrodes

Marimo-like graphene (MG) was made from MCMB powder mixed with KOH flakes (mass ratio 1:5) for 1 hat  $1000\text{ }^\circ\text{C}$  muffle furnace [56]. After treatment and removal of KOH,  $60\text{ mg}$  MG was dispersed into  $10\text{ mL}$  of DI water and then ultrasonically dispersed for  $30\text{ min}$ .  $\text{HAuCl}_4$  and the ascorbic acid solution were prepared by adding  $6\text{ mg}$  of  $\text{HAuCl}_4$  into  $5\text{ mL}$  of DI water and  $30\text{ mg}$  of ascorbic acid into  $5\text{ mL}$  of DI water, respectively.  $10\text{ mL}$  MG water dispersion was mixed with the  $\text{HAuCl}_4$  and ascorbic acid solution, followed by stirring for  $30\text{ min}$  using a magnetic stirrer. After that, the solid product was filtered from dispersion and rinsed with DI water three times. The solid product is Au NP/MG [57]. The Au NP/MG was redispersed in DI water to obtain  $3\text{ mg mL}^{-1}$  dispersion for the next modification step.

GCE electrodes with a diameter of  $3\text{ mm}$  (geometric area:  $7.07\text{ mm}^2$ ) were applied as the substrate electrodes. Before modification, GCE electrodes were polished using  $0.05\text{ }\mu\text{m}$  alumina slurry and cleaned in deionized water and ethanol by ultrasonication. Following that, GCE was activated via 100 times cyclic voltammetric scanning in  $0.5\text{ M H}_2\text{SO}_4$  with a potential range from  $-1.0$  to  $1.0\text{ V vs. SCE}$  and a scan rate of  $100\text{ mV s}^{-1}$ .  $6\text{ }\mu\text{L}$  of Au NP/MG aqueous dispersion was drop-casted to the center of the GCE. After drying at  $60\text{ }^\circ\text{C}$  for  $10\text{ min}$ , Au NP/MG/GCE was finally fabricated. MCMB/GCE, MG/GCE, and Au NP/MCMB/GCE electrodes were prepared as similar method.

### 2.3. Samples Preparation

We diluted  $10\times$  PBS 10 times using DI water to obtain  $1\times$  PBS, which was adopted as a buffer solution. The  $20\text{ }\mu\text{M}$  DA solution was prepared by adding  $0.038\text{ g}$  of DA into  $100\text{ mL}$  of  $1\times$  PBS, and the DA solutions with lower concentrations were all obtained by

diluting 20  $\mu\text{M}$  DA solution using  $1\times$  PBS in the proper proportion. Gradually adding 1 M KOH solution or 0.5 M  $\text{H}_2\text{SO}_4$  solution ( $1\times$  PBS used as solvent) into 20  $\mu\text{M}$  DA solution to adjust the pH and adding  $1\times$  PBS to adjust DA concentration as well; finally, the solutions with 10  $\mu\text{M}$  DA with different pH from 3 to 11 were obtained for pH study. Real samples were prepared by spiking DA solution with different concentrations into 20 mL of goat serum. The pH of real samples is 7.

#### 2.4. Dopamine Electrochemical Determination

The bare GCE, MCMB/GCE, MG/GCE, Au NP/MCMB/GCE, and Au NP/MG/GCE were applied as working electrodes. A saturated calomel electrode (SCE) and a Pt electrode were applied as reference and counter electrodes, respectively. CV and DPV tests were conducted to analyze the electrochemical behavior of different concentrations of DA on the modified GCE. CV curves (five cycles) were recorded from  $-0.2$  to  $0.4$  V with a scan rate of  $100\text{ mV s}^{-1}$ , whereas DPV tests were conducted from  $-0.2$  to  $0.4$  V with an increment step of 4 mV, amplitude of 50 mV, pulse period of 0.5 s, and pulse duration time is 0.05 s.

#### 2.5. Characterizations

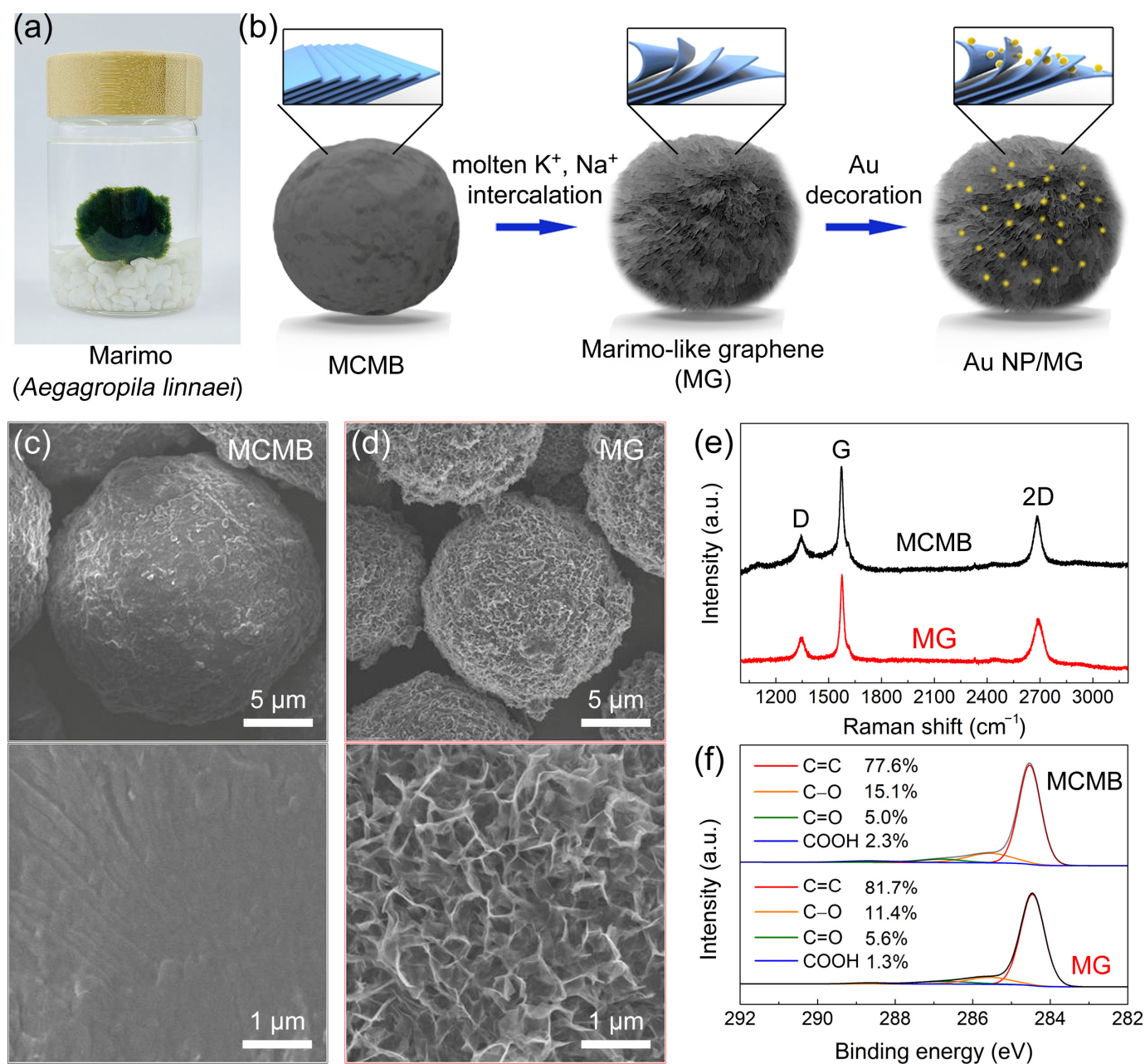
Field emission scanning electron microscope (FEI, Hillsboro, OR, USA) and high-resolution transmission electron microscope (JEOL, Tokyo, Japan) were applied to observe the modified material. Raman spectroscopy (Renishaw PLC, Wotton-under-Edge, UK) with a laser wavelength of 532 nm and X-ray photoelectron spectroscopy (XPS, Kratos Analytical, Manchester, UK) were used to characterize the chemical compositions and element chemical states. All the electrochemical experiments were carried out by a CHI660e electrochemical workstation (Shanghai Chenhua, Shanghai, China).

### 3. Results and Discussion

#### 3.1. Characterization of MG and Au NP/MG

Figure 1a,b show a schematic of the fabrication of marimo-like graphene (MG) and Au nanoparticles-decorated marimo-like graphene (Au NP/MG). The MCMB was mixed with five times the mass of the KOH solid. After raising the temperature to  $1000\text{ }^\circ\text{C}$ , the molten  $\text{K}^+$  ion intercalated into the graphite layer structure of MCMB, forming the partially exfoliated structure. Since the partially exfoliated MCMB is in a spherical shape with a fluffy graphene nanowalls shell, it was named marimo-like graphene (MG) in this work. Au nanoparticles-decorated marimo-like graphene (Au NP/MG) was acquired by decorating gold nanoparticles onto MG in a simple solution method through reducing chloraureate.

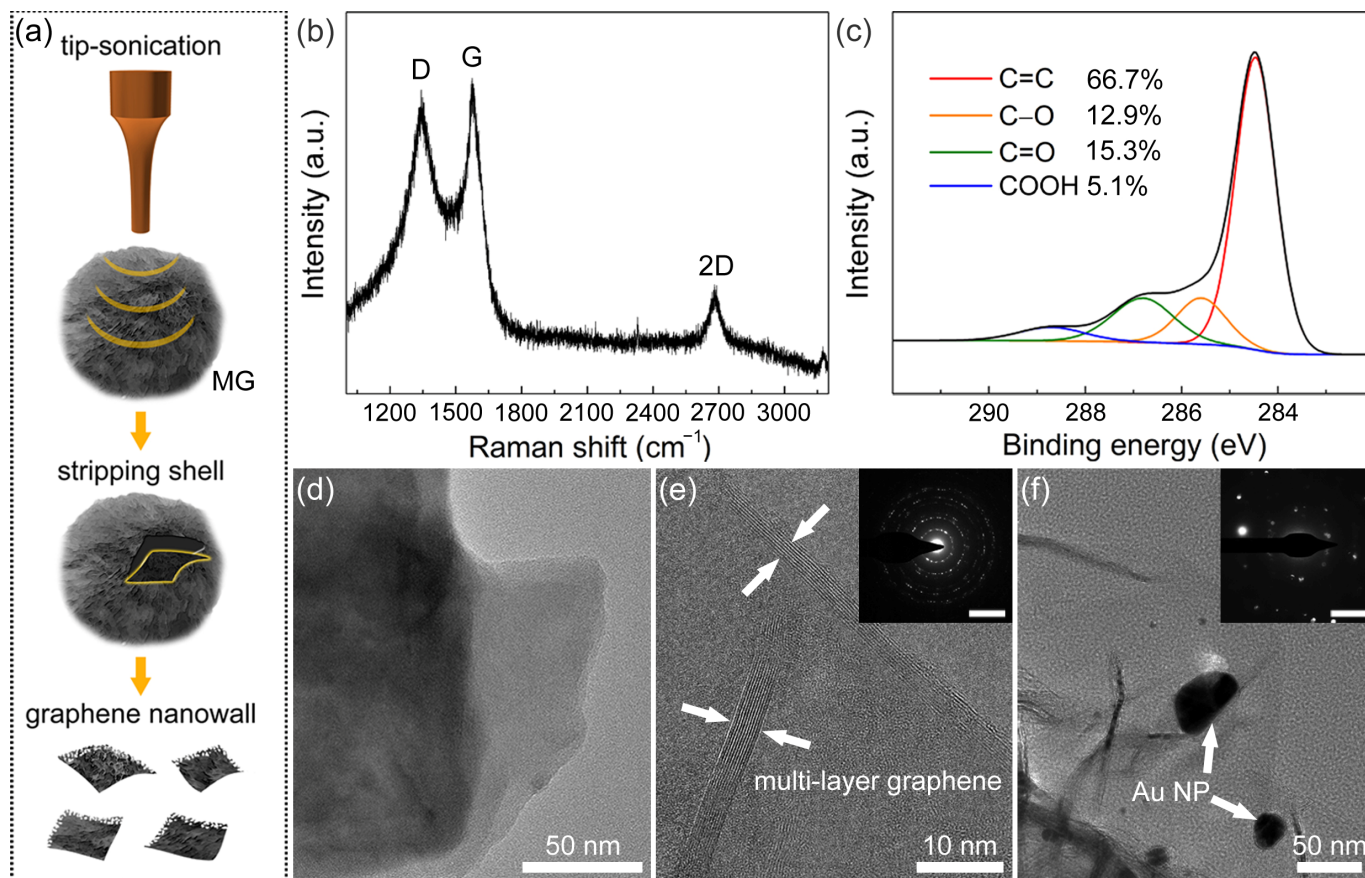
SEM images of MCMB and MG were shown in Figure 1c,d. The MCMB shows a relatively smooth spherical structure, whereas the MG is distinguishably rough. Under high resolution, the rough surface of MG is composed of graphene nanowalls, which were partially exfoliated by molten alkali intercalation [56]. The average diameter of MG is  $\approx 15\text{ }\mu\text{m}$ , which is smaller than that of MCMB ( $\approx 20\text{ }\mu\text{m}$ ). The volume decrease can be attributed to the carbon etching by molten alkali at high temperatures. The Raman spectra of MCMB and MG are shown in Figure 1e. The Raman peaks correspond to the characteristic D-band ( $\approx 1349\text{ cm}^{-1}$ ), G-band ( $\approx 1578\text{ cm}^{-1}$ ), and 2D-band ( $\approx 2698\text{ cm}^{-1}$ ) [58]. Moreover, the  $I_{\text{D}}/I_{\text{G}}$  ratio is 0.27–0.32 and  $I_{2\text{D}}/I_{\text{G}}$  ratio is 0.55–0.65, confirming that their main component is graphite. The high-resolution C1s XPS spectra of MCMB and MG are shown in Figure 1f. The curve results can be fitted into four deconvoluted components:  $\text{sp}^2$ -hybridized bonds (C=C, at  $\approx 284.4\text{ eV}$ ), hydroxyl (C–O, at  $\approx 286.1\text{ eV}$ ), carbonyl (C=O, at  $\approx 287.1\text{ eV}$ ), and carboxylate group (COOH, at  $\approx 288.7\text{ eV}$ ) [27]. The ratio of oxygen-containing groups is 18–23%, and scarcely  $\text{sp}^3$ -hybridized bond (C–C) was found, suggesting that the chemical composition of MCMB and MG is close to pristine graphite [59].



**Figure 1.** (a) Real photo of Marimo. (b) Schematic illustration of the fabrication of Marimo-like graphene (MG) and Au NP-decorated Marimo-like graphene (Au NP/MG). SEM images of (c) MCMB and (d) MG. (e) Raman spectra and (f) C1s XPS spectra of MCMB and MG.

However, compared to the particle size of MG, the thickness of the graphene nanowalls shell is limited. It should be noticed that the results of Raman and XPS spectra in Figure 1e,f reflect the information of the whole MG rather than the graphene nanowalls on the surface. Therefore, the graphene nanowalls shell was stripped from MG by tipsonication and collected for characterization (Figure 2a). As shown in the Raman spectrum of Figure 2b, a remarkable D-band can be observed, and the  $I_D/I_G$  ratio is  $\approx 0.96$ , indicating that a large number of defects exist in the graphene nanowalls shell [60]. These defects are mainly attributed to the exposed edge of graphene nanowalls. The C1s XPS spectrum in Figure 2c can be fitted as the same components as Figure 1f, and the ratio of oxygen-containing groups rose to  $\approx 33\%$ . The increase of oxygen-containing groups is the result of the inevitable oxidation reaction between MCMB and oxygenated compounds (e.g.,  $OH^-$ ,  $O_2$ , and  $H_2O$ )

during molten alkali intercalation. These oxygen-containing groups partially contribute to the defects in the graphene nanowalls shell as well.



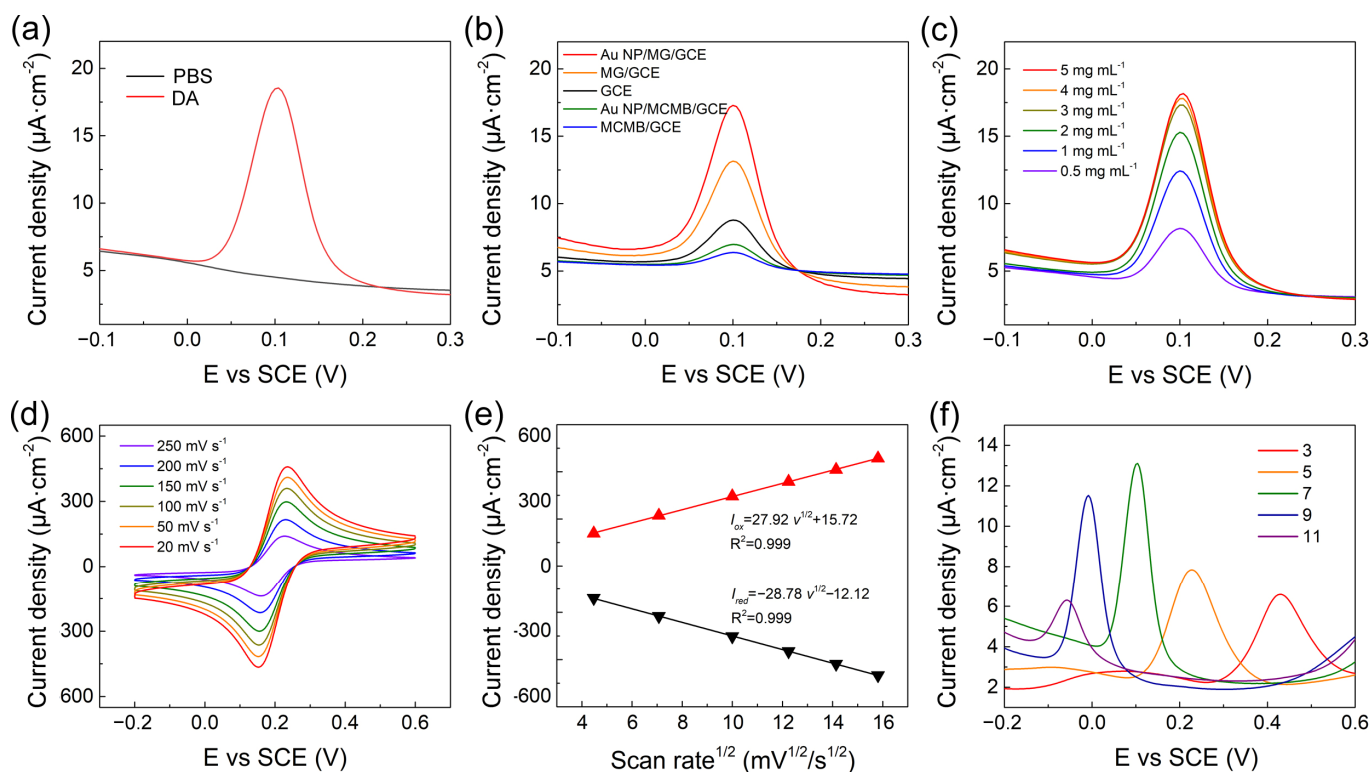
**Figure 2.** (a) Scheme of stripping and collecting graphene nanowalls shell from MG. (b) Raman spectrum and (c) C1s XPS spectrum of graphene nanowalls. (d) TEM image and (e) HRTEM image of MG (inset: SAED pattern; scale bar: 5 nm<sup>-1</sup>). (f) TEM image of Au NP/MG (inset: SAED pattern; scale bar: 5 nm<sup>-1</sup>).

Figure 2d displays the TEM bright field image of the top end of the graphene nanowalls shell. It can be observed that graphene nanowalls consist of a stacked laminated graphene structure. In the HRTEM image (Figure 2e), there are 10 lines of contrast at the edge of the graphene nanowalls shell, indicating that the layer number of multilayered graphene is 10 in this region. The interplanar spacing is approximately 0.34 nm, which corresponds to that of the graphite (002) facet [61]. The corresponding SAED pattern of graphene nanowalls is shown in Figure 2e. The presence of multiple spots revealed that graphene nanowalls are polycrystalline with various rotational stacking angles. In the TEM image of Au NP/MG (Figure 2f), several Au NPs decorate the graphene nanowalls, with a diameter range of 10–40 nm. Meanwhile, the corresponding SAED pattern shows that the Au NPs exist in polycrystalline form.

### 3.2. Au NP/MG/GCE Electrode Performance Optimization of DA Detection

To explore the electrochemical performance of Au NP/MG/GCE towards DA, the DPV technique was conducted on the Au NP/MG/GCE electrodes in PBS with 10 μM DA. Compared to the curve from blank PBS, an oxidation peak at potential position 0.10 V appeared in the experimental group and specified as the characteristic peak for electrochemical analysis of DA, as shown in Figure 3a. As shown in Figure 3b, DPV curves of electrochemical behaviors at a potential interval of −0.1–0.3 V were performed in the presence of 10 μM DA on bare GCE, MCMB/GCE, Au NP/MCMB/GCE, MG/GCE,

and Au NP/MG/GCE electrodes, respectively. The current intensities of MCMB/GCE and Au NP/MCMB/GCE electrodes were both lower than bare GCE, demonstrating the poor electrochemical activity and absorbability of MCMB towards DA. It is noticed that the current density is calculated from the geometric area of GCE. Compared to the MCMB/GCE electrodes, the current intensity of MG/GCE electrodes improved by  $\approx 20\%$ , indicating the much better electrochemical activity of MG than MCMB towards DA. It can be speculated that the specific surface area was greatly enhanced, and lots of edge defects as electrochemical active sites were exposed during the transition of MCMB to MG via molten alkali intercalation [56,62]. After hybridization with Au NPs, the electrochemical performance of Au NP/MG/GCE electrodes improved to the maximum, indicating that the electrodes with better electrical conductivity promoted the electron transfer of the DA oxidation reaction.



**Figure 3.** (a) DPV of Au NP/MG/GCE electrodes with and without 10  $\mu\text{M}$  DA in PBS. (b) DPV curves of various modified electrodes with 10  $\mu\text{M}$  DA in PBS. (c) DPV of Au NP/MG/GCE electrodes with various concentrations of MG to the same of AuNP with 10  $\mu\text{M}$  DA in PBS. (d) Au NP/MG/GCE electrodes in 10 mM  $[\text{Fe}(\text{CN})_6]^{3-/4-}$  and 0.1 M KCl electrolyte solution at scan rates from 20 to 250  $\text{mV s}^{-1}$ . (e) Linear plots of  $I_{ox}/I_{red}$  versus scan rates (f) DPV of 10  $\mu\text{M}$  DA on Au NP/MG/GCE electrodes with pH.

To further improve the electrochemical performance of the proposed sensor, experimental parameters including the preparation of modified electrodes, scan rate, and electrolyte pH were optimized. To confirm the suitable mass of MG in the fabrication of Au NP/MG/GCE electrodes, various concentrations of MG varying from 0.5–5  $\text{mg mL}^{-1}$  at 0.5  $\mu\text{L}$  volume were drop-casted on GCE and dried to perform DPV response in PBS with 10  $\mu\text{M}$  DA. As shown in Figure 3c, the MG concentration was selected as 3  $\text{mg mL}^{-1}$ . The electrochemical behavior of various electrodes was performed by CV in 10 mM  $[\text{Fe}(\text{CN})_6]^{3-/4-}$  containing 0.1 M KCl electrolyte solution at scan rates ranging from 20 to 200  $\text{mVs}^{-1}$  (Figure 3d). The peak currents density of  $I_{ox}$  and  $I_{red}$  both increased linearly with the square root of scan rates (Figure 3e), demonstrating that the redox reaction on the Au NP/MG/GCE electrodes was controlled by diffusion. The effect of pH on the electrochemical response of Au NP/MG/GCE electrodes was performed in the range from 3 to

11 with an increase factor of 2, as shown in Figure 3f. The peak potential position shifted negatively with the increased electrolyte pH, due to an improvement in the deprotonation reaction of DA [63]. The maximum value of peak current is at pH 7 and was chosen as the optimal pH. A possible mechanism of the maximum peak at pH 7 is the combination of the ion concentration effect and electrode surface adsorption process. When  $\text{pH} < 7$ , excess protons ( $\text{H}^+$ ) in the solution will inhibit the deprotonation reaction of DA. When  $\text{pH} > 7$ , DA molecules are negatively charged, and the electrode surface is also negatively charged due to the oxygen-containing group of MG. Therefore, although the deprotonation reaction of DA is promoted, the repelling effect of charge interaction makes it difficult for DA adsorption on the electrode, resulting in the decrease of electrochemical response current.

### 3.3. Electrochemical Determination of DA with Different Concentrations

The quantitative electrochemical determination of DA on the MG/GCE and Au NP/MG/GCE electrodes was performed by DPV measurements, respectively, as presented in Figure 4a,b. The peak current value on the MG/GCE and Au NP/MG/GCE electrodes both enhanced with the increasing concentration of DA. As indicated in Figure 4c, the calibration curve of DA on the MG/GCE and Au NP/MG/GCE electrodes was concluded from the average of peak current value, and the linear range of DA determination was in a range of 0.2–10  $\mu\text{M}$  and 0.02–10  $\mu\text{M}$ . The linear regression equation on the MG/GCE electrodes was  $I_{ox}(\mu\text{A}) = 1.02c(\mu\text{M}) + 2.30$  ( $R^2 = 0.992$ ), and the linear regression equation on the Au NP/MG/GCE electrodes was  $I_{ox}(\mu\text{A}) = 1.51c(\mu\text{M}) + 4.47$  ( $R^2 = 0.997$ ). The limit of detection (LOD) of DA on the MG/GCE and Au NP/MG/GCE electrodes was determined as 0.15  $\mu\text{M}$  and 0.016  $\mu\text{M}$ , respectively. Specifically, the DA determination experiments were performed by the DPV technique on six individual electrodes. Compared with other DA electrochemical sensors focusing on graphene-based modified electrodes, as listed in Table 1, our Au NP/MG/GCE electrodes achieved a relatively low detection LOD of DA with efficiency.

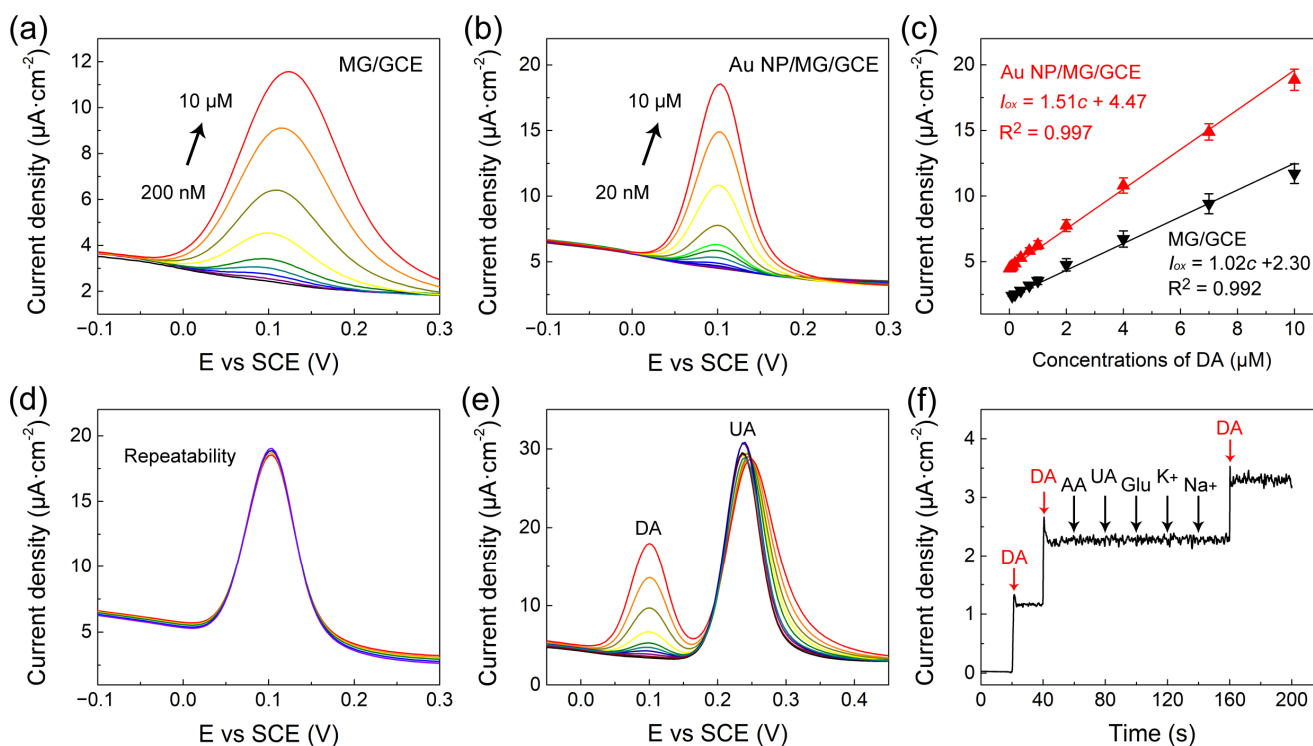


**Figure 4.** (a,b) DPV curves of MG/GCE and Au NP/MG/GCE electrodes with various concentrations of DA, respectively. (c) The corresponding peak current versus DA concentration. (d–f) The repeatability and good anti-interference of Au NP/MG/GCE electrodes.

**Table 1.** Comparison of linear range and detection limit with other graphene-based DA electrochemical sensors.

Modifiers	Decoration	Substrate	Measurements	Linear Range ( $\mu\text{M}$ )	LOD ( $\mu\text{M}$ )	Ref
Graphene sheets		GCE	Amperometry	5.0–710	2.0	[35]
rGO		GCE	DPV	0.5–60	0.50	[47]
rGO		screen-printed electrode	DPV	0.5–2000	0.12	[48]
rGO nanoribbons		screen-printed electrode	DPV	0.5–300	0.15	[64]
rGO	Au NPs	GCE	DPV	6.8–41	1.4	[65]
rGO	Ag NPs	GCE	DPV	10–70	1.0	[29]
rGO	Pt NPs	GCE	DPV	0.03–8.13	0.03	[66]
rGO	Pd–Pt NPs	GCE	DPV	4–200	0.04	[67]
rGO	Au–Pt nanoclusters	GCE	DPV	0.07–49,800	0.02	[68]
Marimo-like graphene	-	GCE	DPV	0.2–100	0.15	This work
Marimo-like graphene	Au NPs	GCE	DPV	0.02–10	0.016	This work

### 3.4. Repeatability, Anti-Interference, Recovery, and Real Sample Analysis

To evaluate the repeatability of Au NP/MG/GCE electrodes for DA determination (10  $\mu\text{M}$ ), DPV curves at a potential interval of  $-0.1$ – $0.3$  V were repeatedly measured 10 times on the same electrodes. As presented in Figure 4d, the oxidation peak potential of DPV curves was consistent at 0.10 V, and the curves overlapped well. The relative standard deviation (RSD) of peak currents was  $\approx 2.6\%$ , indicating good repeatability of Au NP/MG/GCE electrodes. The anti-interference of Au/MG/GCE electrodes in the presence of 20  $\mu\text{M}$  UA as interfering substances was experimented with by DPV curves in goat serum real samples with spiked DA in the range from 0.1 to 10  $\mu\text{M}$ , as indicated in Figure 4e. Compared to the values of the calibration curve in Figure 4c, the anti-interference results indicated that the presence of UA did not intervene in DA determination. Furthermore, the anti-interference of Au NP/MG/GCE electrodes in the presence of other potential interfering substances such as 1  $\mu\text{M}$  ascorbic acid (AA), 1  $\mu\text{M}$  glucose (Glu), 1  $\mu\text{M}$  UA, 1  $\mu\text{M}$   $\text{K}^+$ , and 1  $\mu\text{M}$   $\text{Na}^+$  in  $1 \times$  PBS containing 0.1  $\mu\text{M}$  DA was conducted by chronoamperometry measurements, as presented in Figure 4f. The results demonstrated that our constructed sensors have good anti-interference against other molecules during electrochemical determination. The standard addition method was applied to verify the recovery property of Au NP/MG/GCE electrodes. DPV curves of spiked serum samples with different DA concentrations (0.12–7.6  $\mu\text{M}$ ) were recorded under optimal conditions. As shown in Table 2, the prepared DA sensor exhibited good recoveries (99.7–106.5%) and low RSD values (0.82–1.54%), showing great potential for practical applications.

**Table 2.** Recovery results of DA in real samples by using Au NP/MG/GCE electrodes.

Samples	Added ( $\mu\text{M}$ )	Founded ( $\mu\text{M}$ )	RSD (%)	Recovery (%)
Goat serum	0.120	0.123	1.06	102.5
	0.740	0.784	1.18	106.0
	1.30	1.38	1.54	106.2
	3.70	3.94	1.40	106.5
	7.60	7.58	0.82	99.7

## 4. Conclusions

In this work, a DA sensor based on an Au NP/MG/GCE electrode was proposed. MG was prepared through partial exfoliation commercial MCMB via molten alkali intercalation.

The exfoliated graphene nanowalls structure on MG microbeads not only increases specific surface area but also provides numerous electrochemical active sites. Compared to MCMB-based electrodes, MG-based electrodes display high sensitivity toward the oxidation of DA molecules. With the assistance of Au NP, the Au NP/MG/GCE electrode exhibited optimized properties for DA determination with a wide linear range from 0.02 to 10  $\mu\text{M}$  and an ultralow detection limit of 0.016  $\mu\text{M}$ . The good recovery (99.7–106.5%) and practicability of Au NP/MG/GCE electrode for DA detection in a real sample have been validated in goat serum samples. Moreover, the anti-interference of Au NP/MG/GCE electrode was further investigated by spiking other biological molecules and ions. We believe this study can provide a promising pathway to construct an electrochemical sensor based on MCMB derivatives.

**Author Contributions:** Conceptualization, methodology, data curation and writing—original draft, Q.T.; Conceptualization, methodology, writing—review and editing, Y.S.; Methodology, data curation, Y.Z.; Conceptualization, methodology, supervision, D.D.; Methodology, writing—review and editing, M.S.; Software, writing—review & editing, W.C.; Supervision, writing—review & editing, T.C.; Supervision, writing—review and editing, H.-S.T.; Supervision, funding acquisition, H.L.; Supervision, funding acquisition, N.J.; Conceptualization, writing—original draft, L.F.; Methodology, data curation, and supervision, H.X. Data curation, writing—original draft, writing—review and editing, C.Y.; Conceptualization, writing—review and editing, funding acquisition, C.-T.L. All authors have read and agreed to the published version of the manuscript.

**Funding:** The authors are grateful for the financial support from the National Natural Science Foundation of China (52102055, 5227020331, and 52075527), National Key R&D Program of China (2017YFB0406000 and 2017YFE0128600), the Project of the Chinese Academy of Sciences (XDC07030100, XDA22020602, ZDKYYQ20200001, and ZDRW-CN-2019-3), CAS Youth Innovation Promotion Association (2020301), Science and Technology Major Project of Ningbo (2021Z120, 2021Z115, 2022Z084, 2018B10046, and 2016S1002), the Natural Science Foundation of Ningbo (2017A610010), Foundation of State Key Laboratory of Solid Lubrication (LSL-1912), China Postdoctoral Science Foundation (2020M681965 and 2022M713243), National Key Laboratory of Science and Technology on Advanced Composites in Special Environments (6142905192806), and the 3315 Program of Ningbo for financial support.

**Institutional Review Board Statement:** Not applicable.

**Informed Consent Statement:** Not applicable.

**Data Availability Statement:** Data sharing not applicable.

**Conflicts of Interest:** The authors declare no conflict of interest.

## References

1. Love, T.M. Oxytocin, motivation and the role of dopamine. *Pharmacol. Biochem. Behav.* **2014**, *119*, 49–60. [[CrossRef](#)] [[PubMed](#)]
2. Tobler, P.N.; Fiorillo, C.D.; Schultz, W. Adaptive Coding of Reward Value by Dopamine Neurons. *Science* **2005**, *307*, 1642–1645. [[CrossRef](#)] [[PubMed](#)]
3. Berridge, K.C.; Robinson, T.E. What is the role of dopamine in reward: Hedonic impact, reward learning, or incentive salience? *Brain Res. Rev.* **1998**, *28*, 309–369. [[CrossRef](#)] [[PubMed](#)]
4. Decarli, N.O.; Zapp, E.; de Souza, B.S.; Santana, E.R.; Winiarski, J.P.; Vieira, I.C. Biosensor based on laccase-halloysite nanotube and imidazolium zwitterionic surfactant for dopamine determination. *Biochem. Eng. J.* **2022**, *186*, 108565. [[CrossRef](#)]
5. Porter, E.; Roussakis, A.-A.; Lao-Kaim, N.P.; Piccini, P. Multimodal dopamine transporter (DAT) imaging and magnetic resonance imaging (MRI) to characterise early Parkinson's disease. *Park. Relat. Disord.* **2020**, *79*, 26–33. [[CrossRef](#)]
6. Martorana, A.; Di Lorenzo, F.; Esposito, Z.; Giudice, T.L.; Bernardi, G.; Caltagirone, C.; Koch, G. Dopamine D2-agonist Rotigotine effects on cortical excitability and central cholinergic transmission in Alzheimer's disease patients. *Neuropharmacology* **2012**, *64*, 108–113. [[CrossRef](#)]
7. Cernat, A.; Ștefan, G.; Tertis, M.; Cristea, C.; Simon, I. An overview of the detection of serotonin and dopamine with graphene-based sensors. *Bioelectrochemistry* **2020**, *136*, 107620. [[CrossRef](#)]
8. Rusheen, A.E.; Gee, T.A.; Jang, D.P.; Blaha, C.D.; Bennet, K.E.; Lee, K.H.; Heien, M.L.; Oh, Y. Evaluation of electrochemical methods for tonic dopamine detection in vivo. *TrAC Trends Anal. Chem.* **2020**, *132*, 116049. [[CrossRef](#)]
9. Zhao, H.-X.; Mu, H.; Bai, Y.-H.; Yu, H.; Hu, Y.-M. A rapid method for the determination of dopamine in porcine muscle by pre-column derivatization and HPLC with fluorescence detection. *J. Pharm. Anal.* **2011**, *1*, 208–212. [[CrossRef](#)]

10. Gao, W.; Qi, L.; Liu, Z.; Majeed, S.; Kitte, S.A.; Xu, G. Efficient lucigenin/thiourea dioxide chemiluminescence system and its application for selective and sensitive dopamine detection. *Sens. Actuators B Chem.* **2017**, *238*, 468–472. [[CrossRef](#)]
11. Zhao, Y.; Zhao, S.; Huang, J.; Ye, F. Quantum dot-enhanced chemiluminescence detection for simultaneous determination of dopamine and epinephrine by capillary electrophoresis. *Talanta* **2011**, *85*, 2650–2654. [[CrossRef](#)] [[PubMed](#)]
12. Sharma, A.; Tok, A.I.Y.; Alagappan, P.; Liedberg, B. Point of care testing of sports biomarkers: Potential applications, recent advances and future outlook. *TrAC Trends Anal. Chem.* **2021**, *142*, 116327. [[CrossRef](#)]
13. Zhang, B.; Chen, M.; Cao, J.; Liang, Y.; Tu, T.; Hu, J.; Li, T.; Cai, Y.; Li, S.; Liu, B.; et al. An integrated electrochemical POCT platform for ultrasensitive circRNA detection towards hepatocellular carcinoma diagnosis. *Biosens. Bioelectron.* **2021**, *192*, 113500. [[CrossRef](#)]
14. Emran, M.Y.; Shenashen, M.A.; Eid, A.I.; Selim, M.M.; El-Safty, S.A. Portable sensitive and selective biosensing assay of dopamine in live cells using dual phosphorus and nitrogen doped carbon urchin-like structure. *Chem. Eng. J.* **2021**, *430*, 132818. [[CrossRef](#)]
15. Zaki, M.F.; Chen, P.-C.; Yeh, Y.-C.; Lin, P.-H.; Xu, M.-Y. Engineering a monolithic 3D paper-based analytical device ( $\mu$ PAD) by stereolithography 3D printing and sequential digital masks for efficient 3D mixing and dopamine detection. *Sens. Actuators A Phys.* **2022**, *347*, 113991. [[CrossRef](#)]
16. Stuart, T.; Jeang, W.J.; Slivicki, R.A.; Brown, B.J.; Burton, A.; Brings, V.E.; Alarcón-Segovia, L.C.; Agyare, P.; Ruiz, S.; Tyree, A.; et al. Wireless, Battery-Free Implants for Electrochemical Catecholamine Sensing and Optogenetic Stimulation. *ACS Nano* **2022**, *17*, 561–574. [[CrossRef](#)]
17. Sajid, M.; Nazal, M.K.; Mansha, M.; Alsharaa, A.; Jillani, S.M.S.; Basheer, C. Chemically modified electrodes for electrochemical detection of dopamine in the presence of uric acid and ascorbic acid: A review. *TrAC Trends Anal. Chem.* **2015**, *76*, 15–29. [[CrossRef](#)]
18. Sajid, M.; Baig, N.; Alhooshani, K. Chemically modified electrodes for electrochemical detection of dopamine: Challenges and opportunities. *TrAC Trends Anal. Chem.* **2019**, *118*, 368–385. [[CrossRef](#)]
19. Niwa, O.; Jia, J.; Sato, Y.; Kato, D.; Kurita, R.; Maruyama, K.; Suzuki, K.; Hirono, S. Electrochemical Performance of Angstrom Level Flat Sputtered Carbon Film Consisting of  $sp^2$  and  $sp^3$  Mixed Bonds. *J. Am. Chem. Soc.* **2006**, *128*, 7144–7145. [[CrossRef](#)]
20. Chiavazza, E.; Berto, S.; Giacomino, A.; Malandrino, M.; Barolo, C.; Prenesti, E.; Vione, D.; Abollino, O. Electrocatalysis in the oxidation of acetaminophen with an electrochemically activated glassy carbon electrode. *Electrochim. Acta* **2016**, *192*, 139–147. [[CrossRef](#)]
21. Arumugam, B.; Muthukutty, B.; Chen, S.-M.; Ramaraj, S.K.; Kumar, J.V.; Nagarajan, E.R. Ultrasonication-aided synthesis of nanoplates-like iron molybdate: Fabricated over glassy carbon electrode as an modified electrode for the selective determination of first generation antihistamine drug promethazine hydrochloride. *Ultrason. Sonochem.* **2020**, *66*, 104977. [[CrossRef](#)] [[PubMed](#)]
22. Oloketuyi, S.; Mazzega, E.; Zavašnik, J.; Pungjunun, K.; Kalcher, K.; de Marco, A.; Mehmeti, E. Electrochemical immunosensor functionalized with nanobodies for the detection of the toxic microalgae *Alexandrium minutum* using glassy carbon electrode modified with gold nanoparticles. *Biosens. Bioelectron.* **2020**, *154*, 112052. [[CrossRef](#)] [[PubMed](#)]
23. Chen, G.; Wang, Z.; Yang, T.; Huang, D.; Xia, D. Electrocatalytic Hydrogenation of 4-Chlorophenol on the Glassy Carbon Electrode Modified by Composite Polypyrrole/Palladium Film. *J. Phys. Chem. B* **2006**, *110*, 4863–4868. [[CrossRef](#)] [[PubMed](#)]
24. Hammoud, A.; Chhin, D.; Nguyen, D.K.; Sawan, M. A new molecular imprinted PEDOT glassy carbon electrode for carbamazepine detection. *Biosens. Bioelectron.* **2021**, *180*, 113089. [[CrossRef](#)] [[PubMed](#)]
25. Xu, T.; Song, Y.; Gao, W.; Wu, T.; Xu, L.-P.; Zhang, X.; Wang, S. Superwetable Electrochemical Biosensor toward Detection of Cancer Biomarkers. *ACS Sens.* **2018**, *3*, 72–78. [[CrossRef](#)]
26. Shi, Z.; Huang, H.; Wang, C.; Huo, M.; Ho, S.-H.; Tsai, H.-S. Heterogeneous transition metal dichalcogenides/graphene composites applied to the metal-ion batteries. *Chem. Eng. J.* **2022**, *447*, 137469. [[CrossRef](#)]
27. Loan, P.T.K.; Wu, D.; Ye, C.; Li, X.; Tra, V.T.; Wei, Q.; Fu, L.; Yu, A.; Li, L.-J.; Lin, C.-T. Hall effect biosensors with ultraclean graphene film for improved sensitivity of label-free DNA detection. *Biosens. Bioelectron.* **2018**, *99*, 85–91. [[CrossRef](#)]
28. Gao, J.; Yuan, Q.; Ye, C.; Guo, P.; Du, S.; Lai, G.; Yu, A.; Jiang, N.; Fu, L.; Lin, C.-T.; et al. Label-Free Electrochemical Detection of Vanillin through Low-Defect Graphene Electrodes Modified with Au Nanoparticles. *Materials* **2018**, *11*, 489. [[CrossRef](#)]
29. Nayak, S.P.; Ramamurthy, S.S.; Kumar, J.K.K. Green synthesis of silver nanoparticles decorated reduced graphene oxide nanocomposite as an electrocatalytic platform for the simultaneous detection of dopamine and uric acid. *Mater. Chem. Phys.* **2020**, *252*, 123302. [[CrossRef](#)]
30. Fu, C.; Sun, Y.; Huang, C.; Wang, F.; Li, N.; Zhang, L.; Ge, S.; Yu, J. Ultrasensitive sandwich-like electrochemical biosensor based on core-shell Pt@CeO<sub>2</sub> as signal tags and double molecular recognition for cerebral dopamine detection. *Talanta* **2020**, *223*, 121719. [[CrossRef](#)]
31. Zhang, W.; Sharma, G.; Kumar, A.; Shekh, M.I.; Stadler, F.J. Fabrication and characterization of Ni/Ag/Zn trimetal oxide nanocomposites and its application in dopamine sensing. *Mater. Today Commun.* **2021**, *29*, 102726. [[CrossRef](#)]
32. Sun, C.-L.; Lai, S.-Y.; Tsai, K.-J.; Wang, J.; Zhou, J.; Chen, H.-Y. Application of nanoporous core-shell structured multi-walled carbon nanotube-graphene oxide nanoribbons in electrochemical biosensors. *Microchem. J.* **2022**, *179*, 107586. [[CrossRef](#)]
33. Yue, H.Y.; Huang, S.; Chang, J.; Heo, C.; Yao, F.; Adhikari, S.; Güneş, F.; Liu, L.; Lee, T.H.; Oh, E.S.; et al. ZnO Nanowire Arrays on 3D Hierarchical Graphene Foam: Biomarker Detection of Parkinson's Disease. *ACS Nano* **2014**, *8*, 1639–1646. [[CrossRef](#)]
34. Mariyappan, V.; Jeyapragasam, T.; Chen, S.-M.; Murugan, K. Mo-W-O nanowire intercalated graphene aerogel nanocomposite for the simultaneous determination of dopamine and tyrosine in human urine and blood serum sample. *J. Electroanal. Chem.* **2021**, *895*, 115391. [[CrossRef](#)]

35. Qi, S.; Zhao, B.; Tang, H.; Jiang, X. Determination of ascorbic acid, dopamine, and uric acid by a novel electrochemical sensor based on pristine graphene. *Electrochim. Acta* **2015**, *161*, 395–402. [[CrossRef](#)]
36. Zhu, Y.; Tian, Q.; Li, X.; Wu, L.; Yu, A.; Lai, G.; Fu, L.; Wei, Q.; Dai, D.; Jiang, N.; et al. A Double-Deck Structure of Reduced Graphene Oxide Modified Porous  $Ti_3C_2T_x$  Electrode towards Ultrasensitive and Simultaneous Detection of Dopamine and Uric Acid. *Biosensors* **2021**, *11*, 462. [[CrossRef](#)]
37. Zou, H.L.; Li, B.L.; Luo, H.Q.; Li, N.B. 0D-2D heterostructures of Au nanoparticles and layered MoS<sub>2</sub> for simultaneous detections of dopamine, ascorbic acid, uric acid, and nitrite. *Sens. Actuators B Chem.* **2017**, *253*, 352–360. [[CrossRef](#)]
38. Tian, J.; Cao, H.; Wu, W.; Yu, Q.; Chen, Y.P. Direct Imaging of Graphene Edges: Atomic Structure and Electronic Scattering. *Nano Lett.* **2011**, *11*, 3663–3668. [[CrossRef](#)] [[PubMed](#)]
39. Yuan, Q.; Liu, Y.; Ye, C.; Sun, H.; Dai, D.; Wei, Q.; Lai, G.; Wu, T.; Yu, A.; Fu, L.; et al. Highly stable and regenerative graphene–diamond hybrid electrochemical biosensor for fouling target dopamine detection. *Biosens. Bioelectron.* **2018**, *111*, 117–123. [[CrossRef](#)]
40. Jiang, J.; Wang, J.; Wang, P.; Lin, X.; Diao, G. Three-dimensional graphene foams with two hierarchical pore structures for metal-free electrochemical assays of dopamine and uric acid from high concentration of ascorbic acid. *J. Electroanal. Chem.* **2023**, *928*, 117056. [[CrossRef](#)]
41. Zheng, W.; Zhao, X.; Fu, W. Review of Vertical Graphene and its Applications. *ACS Appl. Mater. Interfaces* **2021**, *13*, 9561–9579. [[CrossRef](#)] [[PubMed](#)]
42. Geim, A.K. Graphene: Status and Prospects. *Science* **2009**, *324*, 1530–1534. [[CrossRef](#)] [[PubMed](#)]
43. Fu, L.; Wang, A.; Lai, G.; Su, W.; Malherbe, F.; Yu, J.; Lin, C.-T.; Yu, A. Defects regulating of graphene ink for electrochemical determination of ascorbic acid, dopamine and uric acid. *Talanta* **2018**, *180*, 248–253. [[CrossRef](#)] [[PubMed](#)]
44. Trikaliotis, D.G.; Christoforidis, A.K.; Mitropoulos, A.C.; Kyzas, G.Z. Graphene Oxide Synthesis, Properties and Characterization Techniques: A Comprehensive Review. *Chemengineering* **2021**, *5*, 64. [[CrossRef](#)]
45. Yu, S.; Guo, B.; Zeng, T.; Qu, H.; Yang, J.; Bai, J. Graphene-based lithium-ion battery anode materials manufactured by mechanochemical ball milling process: A review and perspective. *Compos. Part B Eng.* **2022**, *246*, 110232. [[CrossRef](#)]
46. Biranje, P.M.; Patwardhan, A.W.; Joshi, J.B.; Dasgupta, K. Exfoliated graphene and its derivatives from liquid phase and their role in performance enhancement of epoxy matrix composite. *Compos. Part A Appl. Sci. Manuf.* **2022**, *156*, 106886. [[CrossRef](#)]
47. Yang, L.; Liu, D.; Huang, J.; You, T. Simultaneous determination of dopamine, ascorbic acid and uric acid at electrochemically reduced graphene oxide modified electrode. *Sens. Actuators B Chem.* **2014**, *193*, 166–172. [[CrossRef](#)]
48. Ping, J.; Wu, J.; Wang, Y.; Ying, Y. Simultaneous determination of ascorbic acid, dopamine and uric acid using high-performance screen-printed graphene electrode. *Biosens. Bioelectron.* **2012**, *34*, 70–76. [[CrossRef](#)]
49. Ye, C.; Zhang, F.; Tan, X.; Sun, H.; Dai, W.; Yang, K.; Yang, M.; Du, S.; Dai, D.; Yu, J.; et al. A dense graphene monolith with poloxamer prefunctionalization enabling aqueous redispersion to obtain solubilized graphene sheets. *Chin. Chem. Lett.* **2020**, *31*, 2507–2511. [[CrossRef](#)]
50. Tran, T.S.; Dutta, N.K.; Choudhury, N.R. Graphene inks for printed flexible electronics: Graphene dispersions, ink formulations, printing techniques and applications. *Adv. Colloid Interface Sci.* **2018**, *261*, 41–61. [[CrossRef](#)]
51. Tzouvadaki, I.; Aliakbarinodehi, N.; Pineda, D.D.; De Micheli, G.; Carrara, S. Graphene nanowalls for high-performance chemotherapeutic drug sensing and anti-fouling properties. *Sens. Actuators B Chem.* **2018**, *262*, 395–403. [[CrossRef](#)]
52. Du, J.; Ma, J.; Liu, Z.; Wang, W.; Jia, H.; Zhang, M.; Nie, Y. Fabrication of Si@mesocarbon microbead (MCMB) anode based on carbon texture for lithium-ion batteries. *Mater. Lett.* **2022**, *315*, 131921. [[CrossRef](#)]
53. Cheng, Y.; Zhang, Q.; Fang, C.; Guo, S. CVD-Synthesis of MCMB/CNTs Hybrids with Low Specific Surface Area for Supercapacitors. *J. Electrochem. Soc.* **2017**, *164*, A1845–A1851. [[CrossRef](#)]
54. Ji, D.; Liu, Z.; Liu, L.; Low, S.S.; Lu, Y.; Yu, X.; Zhu, L.; Li, C.; Liu, Q. Smartphone-based integrated voltammetry system for simultaneous detection of ascorbic acid, dopamine, and uric acid with graphene and gold nanoparticles modified screen-printed electrodes. *Biosens. Bioelectron.* **2018**, *119*, 55–62. [[CrossRef](#)]
55. Liao, J.; Tian, T.; Shi, S.; Xie, X.; Peng, S.; Zhu, Y.; Xiao, J.; Lin, Y. Broadening the biocompatibility of gold nanorods from rat to *Macaca fascicularis*: Advancing clinical potential. *J. Nanobiotechnol.* **2021**, *19*, 195. [[CrossRef](#)]
56. Xia, H.; Wang, K.; Yang, S.; Shi, Z.; Wang, H.; Wang, J. Formation of graphene flowers during high temperature activation of mesocarbon microbeads with KOH. *Microporous Mesoporous Mater.* **2016**, *234*, 384–391. [[CrossRef](#)]
57. Zhang, J.; Kambayashi, M.; Oyama, M. A novel electrode surface fabricated by directly attaching gold nanospheres and nanorods onto indium tin oxide substrate with a seed mediated growth process. *Electrochem. Commun.* **2004**, *6*, 683–688. [[CrossRef](#)]
58. Li, J.; Qin, Y.; Chen, Y.; Shen, J.; Song, Y.; Wang, Z. Structural characteristics and evolution of meta-anthracite to coaly graphite: A quantitative investigation using X-ray diffraction, Raman spectroscopy, and high-resolution transmission electron microscopy. *Fuel* **2023**, *333*, 126334. [[CrossRef](#)]
59. Al-Gaashani, R.; Najjar, A.; Zakaria, Y.; Mansour, S.; Atieh, M.A. XPS and structural studies of high quality graphene oxide and reduced graphene oxide prepared by different chemical oxidation methods. *Ceram. Int.* **2019**, *45*, 14439–14448. [[CrossRef](#)]
60. Liu, L.; Jia, L.; Huang, Y.; Zhang, Y.; Yu, W. High-performance vertical graphene nanowall/silicon Schottky junction solar cells with Nafion doping and plasma etching. *J. Alloys Compd.* **2023**, *939*, 168765. [[CrossRef](#)]
61. Tu, C.-H.; Chen, W.; Fang, H.-C.; Tzeng, Y.; Liu, C.-P. Heteroepitaxial nucleation and growth of graphene nanowalls on silicon. *Carbon* **2013**, *54*, 234–240. [[CrossRef](#)]

62. Li, J.; Zhang, Y.; Huo, M.; Ho, S.-H.; Tsai, H.-S. Metallic group VB transition metal dichalcogenides for electrochemical energy storage. *Mater. Today Chem.* **2022**, *26*, 101241. [[CrossRef](#)]
63. Guo, Z.; Huang, G.-Q.; Li, J.; Wang, Z.-Y.; Xu, X.-F. Graphene oxide-Ag/poly-l-lysine modified glassy carbon electrode as an electrochemical sensor for the determination of dopamine in the presence of ascorbic acid. *J. Electroanal. Chem.* **2015**, *759*, 113–121. [[CrossRef](#)]
64. Mohammadi, S.; Taher, M.A.; Beitollahi, H. Treated Screen Printed Electrodes Based on Electrochemically Reduced Graphene Nanoribbons for the Sensitive Voltammetric Determination of Dopamine in the Presence of Uric Acid. *Electroanalysis* **2020**, *32*, 2036–2044. [[CrossRef](#)]
65. Wang, C.; Du, J.; Wang, H.; Zou, C.; Jiang, F.; Yang, P.; Du, Y. A facile electrochemical sensor based on reduced graphene oxide and Au nanoplates modified glassy carbon electrode for simultaneous detection of ascorbic acid, dopamine and uric acid. *Sens. Actuators B Chem.* **2014**, *204*, 302–309. [[CrossRef](#)]
66. Sun, C.-L.; Lee, H.-H.; Yang, J.-M.; Wu, C.-C. The simultaneous electrochemical detection of ascorbic acid, dopamine, and uric acid using graphene/size-selected Pt nanocomposites. *Biosens. Bioelectron.* **2011**, *26*, 3450–3455. [[CrossRef](#)]
67. Yan, J.; Liu, S.; Zhang, Z.; He, G.; Zhou, P.; Liang, H.; Tian, L.; Zhou, X.; Jiang, H. Simultaneous electrochemical detection of ascorbic acid, dopamine and uric acid based on graphene anchored with Pd–Pt nanoparticles. *Colloids Surf. B Biointerfaces* **2013**, *111*, 392–397. [[CrossRef](#)] [[PubMed](#)]
68. Liu, Y.; She, P.; Gong, J.; Wu, W.; Xu, S.; Li, J.; Zhao, K.; Deng, A. A novel sensor based on electrodeposited Au–Pt bimetallic nano-clusters decorated on graphene oxide (GO)–electrochemically reduced GO for sensitive detection of dopamine and uric acid. *Sens. Actuators B Chem.* **2015**, *221*, 1542–1553. [[CrossRef](#)]

**Disclaimer/Publisher’s Note:** The statements, opinions and data contained in all publications are solely those of the individual author(s) and contributor(s) and not of MDPI and/or the editor(s). MDPI and/or the editor(s) disclaim responsibility for any injury to people or property resulting from any ideas, methods, instructions or products referred to in the content.